Density functional theory for inhomogeneous mixtures of polymeric fluids

Yang-Xin Yu[a] and Jianzhong Wu[b]
Department of Chemical and Environmental Engineering, University of California, Riverside, California 92521-0425

(Received 19 February 2002; accepted 14 May 2002)

A new density functional theory is developed for inhomogeneous mixtures of polymeric fluids by combining Rosenfeld's fundamental-measure theory for excluded volume effects with Wertheim's first-order thermodynamic perturbation theory for chain connectivity. With no adjustable parameters, theoretical predictions are in excellent agreement with Monte Carlo simulation data for the density distributions and for the adsorption isotherms of hard-sphere chains near hard walls or in slit-like pores. This theory is applied to calculate the force between two parallel hard walls separated by hard-sphere chains at different densities. Calculated results indicate that the chain-mediated force is attractive and decays monotonically with separation at low chain densities, it oscillates at high chain densities and in between, it is attractive at small separation and repulsive at large separation. This new density functional theory is simpler than similar theories in the literature and is directly applicable to mixtures. © *2002 American Institute of Physics.* [DOI: 10.1063/1.1491240]

I. INTRODUCTION

Structural and thermodynamic properties of confined polymeric fluids are of interest in industrial applications such as surface coating, lubrication, adhesion, and colloidal stability.[1–3] Properties of confined polymeric fluids are determined by, in addition to attractive forces arising from polymer segments and surfaces, a competition between excluded volume of individual segments and chain connectivity. The excluded-volume effect is most significant at high densities while chain connectivity dominates polymer properties at low densities.

Whereas the theory of polymer interfaces is now well advanced, the quantitative description of interfacial thermodynamic properties remains challenging. Much difficulty arises from the accurate representation of both chain connectivity and excluded volume effects.[4] For instance, self-consistent-field theory has been remarkably successful at representing chain connectivity but it is only semiquantitative at representing excluded volume effects.[5–8] Alternative approaches include integral-equation theories[9–12] and density functional theories (DFTs).[13–15] Two complementary methods can be used to derive the grand potential in density functional theories: one is based on density expansions and the other is based on weighted densities.[16] For molecular systems, the density expansion approach was first proposed by Chandler, McCoy, and Singer (CMS),[13–15] here referred to as the CMS-DFT approach;[17] the weighted-density approach for chain fluids was initially introduced by Woodward,[18] and by Kierlik and Rosinburg (KR).[19] Because the closure relations in integral-equation theories can also be derived from density expansions, the CMS-DFT approach is closely tied to integral-equation theories.[16]

In KR theory for chain fluids, Wertheim's first-order thermodynamic perturbation (TPT1) theory is applied to represent thermodynamic properties in the bulk limit.[20,21] For engineering applications, TPT1 is attractive because it is relatively simple and compares favorably with simulation results.[22–26] However, numerical implementation of KR theory is inconvenient because to represent chain connectivity, it requires the cavity correlation function of inhomogeneous hard-sphere fluid. Alternatively, Yethiraj and Woodward (YW)[27,28] proposed a density functional theory that combines an exact expression for the free energy of noninteracting chains with a weighted-density approach for the excess free energy functional of hard-sphere chains. This theory requires single-chain density profiles that must be obtained self-consistently from Monte Carlo simulation.

The CMS-DFT approach has also been applied to investigate the structures and thermodynamics of polyatomic fluids.[29–32] In this approach, the direct correlation functions are from molecular integral-equation theory and the intramolecular correlation functions are from a single-chain Monte Carlo simulation. Recently, more efficient methodologies had been proposed for numerical implementations.[33,34] These new methods, that avoid extensive single-chain Monte Carlo simulation, have been successfully applied to predict the density profiles,[17,34] surface excesses, and surface tensions[35] of tangentially connected hard-sphere chains near hard surfaces, and the entropic forces between hard walls separated by hard-sphere chains.[36]

In this paper, we report a new density functional theory for a ''primitive'' model of polymer solutions/melts where polymers are represented by freely jointed hard-sphere chains and solvent molecules are monomeric hard spheres. For direct comparison with molecular simulation results, van der Waals forces are not included. This new density func-

[a]Also at: The Department of Chemical Engineering, Tsinghua University, Beijing 100084, P. R. China.
[b]Author to whom all correspondence should be addressed; electronic mail: jwu@engr.ucr.edu

tional combines the fundamental measure theory (FMT) of Rosenfeld[37] for excluded volume effect and Wertheim's TPT1[21] for chain connectivity. It has been applied to describe the adsorption isotherms, solvation forces, and density profiles of hard-sphere chains and chain-sphere mixtures near a hard wall or in slit pores. Compared with previous theories for confined polymeric fluids, the method reported here has the advantages of simplicity and numerical efficiency. Further, it is directly applicable to mixtures of polymeric fluids.

II. THEORY

A. Density functional for mixtures of hard spheres and hard-sphere chains

We consider a binary mixture of monomeric hard spheres and tangentially connected hard-sphere chains. In a tangentially connected chain, the bond length is equal to the segment diameter σ_1 and there is no angular constraint between neighboring bonds, i.e., each sphere can freely roll over the surface of its immediate neighbor unless it encounters another sphere. In terms of bonding potentials, the chain connectivity is represented by

$$V_b(\mathbf{R}) = \sum_{i=1}^{M-1} \nu_b(|\mathbf{r}_{i+1} - \mathbf{r}_i|), \tag{1}$$

where M stands for the number of segments for each chain, $\mathbf{R} \equiv (\mathbf{r}_1, \mathbf{r}_2, \cdots, \mathbf{r}_M)$ denotes a set of coordinates describing the segmental positions, and ν_b is the bonding potential. For an arbitrary chain configuration (arrangement of segments), the total bonding energy satisfies

$$\exp[-\beta V_b(\mathbf{R})] \propto \prod_{i=1}^{M-1} \delta(|\mathbf{r}_{i+1} - \mathbf{r}_i| - \sigma_1), \tag{2}$$

where β^{-1} is the Boltzmann's constant k_B multiplied by the thermal temperature T, $\delta(r)$ is the Dirac delta function. The quantity $\exp[-\beta V_b(\mathbf{R})]$ represents the probability density of a hard-sphere chain with a configuration $\mathbf{R}$.

The proportionality constant in Eq. (2) can be determined from the normalization condition

$$(1/V) \int \exp[-\beta V_b(\mathbf{R})] d\mathbf{R} = 1, \tag{3}$$

where V is the system volume. Substitution of Eq. (3) into Eq. (2) yields

$$\exp[-\beta V_b(\mathbf{R})] = \prod_{i=1}^{M-1} \frac{\delta(|\mathbf{r}_{i+1} - \mathbf{r}_i| - \sigma_1)}{4\pi\sigma_1^2}. \tag{4}$$

Equation (4) indicates that $\exp[-\beta V_b(\mathbf{R})] = 0$ whenever $|\mathbf{r}_{i+1} - \mathbf{r}_i| \neq \sigma_1$, i.e., whenever two neighboring segments are disconnected or overlapped.

The central goal of a density functional theory is to find an expression for the grand potential Ω, or equivalently, the Helmholtz energy F as a functional of density distributions. For a mixture of hard spheres and hard-sphere chains, the grand potential functional and the Helmholtz energy functional are related via a Legendre transform:

$$\Omega[\rho_M(\mathbf{R}), \rho_2(\mathbf{r})] = F[\rho_M(\mathbf{R}), \rho_2(\mathbf{r})] + \int [\Psi_M(\mathbf{R}) - \mu_M] \rho_M(\mathbf{R}) d\mathbf{R} + \int [\Psi_2(\mathbf{r}) - \mu_2] \rho_2(r) d\mathbf{r}. \tag{5}$$

In Eq. (5), $d\mathbf{R} = d\mathbf{r}_1 d\mathbf{r}_2 \cdots d\mathbf{r}_M$ represents a set of differential volumes, $\rho_M(\mathbf{R})$ is the chain density as a function of segment positions $\mathbf{R}$, $\rho_2(\mathbf{r})$ is the density of hard spheres, μ_M is the chemical potential of a chain molecule, μ_2 is the chemical potential of a hard sphere, and $\Psi_M(\mathbf{R})$ and $\Psi_2(\mathbf{r})$ are, respectively, the external potentials on a chain molecule and on a hard-sphere monomer. The external potential for a chain molecule is equal to the sum of the potential energy on individual segments $\Psi_M(\mathbf{R}) = \Sigma_{i=1}^{M} \varphi_i(\mathbf{r}_i)$.

Once we have an expression for the grand potential $\Omega[\rho_M(\mathbf{R}), \rho_2(\mathbf{r})]$, the equilibrium density distributions satisfy the stationary condition

$$\frac{\delta\Omega}{\delta\rho_M(\mathbf{R})} = \frac{\delta\Omega}{\delta\rho_2(\mathbf{r})} = 0. \tag{6}$$

Solutions to Eq. (6) give the density distributions at equilibrium and subsequently the grand potential and the Helmholtz energy.

B. Helmholtz energy functional

For mixtures of hard spheres and hard-sphere chains, the Helmholtz energy functional $F[\rho_M(\mathbf{R}), \rho_2(\mathbf{r})]$ can be expressed as an ideal gas term $F_{\text{id}}[\rho_M(\mathbf{R}), \rho_2(\mathbf{r})]$ plus an excess term $F_{\text{ex}}[\rho_M(\mathbf{R}), \rho_2(\mathbf{r})]$ due to intra- and intermolecular interactions

$$F[\rho_M(\mathbf{R}), \rho_2(\mathbf{r})] = F_{\text{id}}[\rho_M(\mathbf{R}), \rho_2(\mathbf{r})] + F_{\text{ex}}[\rho_M(\mathbf{R}), \rho_2(\mathbf{r})]. \tag{7}$$

The ideal gas term is known exactly

$$\beta F_{\text{id}} = \int d\mathbf{R} \rho_M(\mathbf{R}) [\ln \rho_M(\mathbf{R}) - 1] + \beta \int d\mathbf{R} \rho_M(\mathbf{R}) V_b(\mathbf{R}) + \int d\mathbf{r}\, \rho_2(\mathbf{r}) [\ln \rho_2(\mathbf{r}) - 1]. \tag{8}$$

Equation (8) is different from that for a mixture of monatomic ideal gases because it includes the bonding potential that takes into account chain connectivity. However, Eq. (8) does not include the excluded volume effect of nonneighboring segments.

To derive the excess Helmholtz energy functional due to intra- and intermolecular interactions, we follow a procedure first proposed by McMullan and Freed (Ref. 4) and more explicitly by Woodward (Ref. 18) where the excess Helmholtz energy is assumed to be a functional of only segment densities. The contribution to the excess Helmholtz energy due to the excluded volume effects is represented by the fundamental-measure theory (FMT) of Rosenfeld.[37] Unlike most other density functional theories, FMT is unique be-

cause it is able to predict the direct correlation function of the corresponding bulk fluid rather than to use it as an input. Besides, it is more accurate than alternative methods for inhomogeneous hard spheres. There are recent improvements over the original FMT but these improvements are targeted for solid phases. Our primarily interest in this work is fluids.

We assume that the excess Helmholtz energy functional can be decomposed as

$$\beta F_{\mathrm{ex}}=\int d\mathbf{r}\{\Phi^{\mathrm{hs}}[n_\alpha(\mathbf{r})]+\Phi^{\mathrm{chain}}[n_\alpha(\mathbf{r})]\}, \tag{9}$$

where $\Phi^{\mathrm{hs}}[n_\alpha(\mathbf{r})]$ and $\Phi^{\mathrm{chain}}[n_\alpha(\mathbf{r})]$ are, respectively, the reduced excess Helmholtz energy densities due to hard-sphere repulsion and chain connectivity. Here the chain connectivity term arises from the indirect interactions due to the exclude volume effects. In contrast, the ideal gas term accounts only the direct bonding potential. Equation (9) implies that the effect of chain connectivity on intramolecular interactions can be accounted for using only segment densities. Following FMT, the scalar and vector weighted densities are defined as

$$n_\alpha(\mathbf{r})=\sum_j n_{\alpha j}(\mathbf{r})=\sum_j \int \rho_j(\mathbf{r}')w_j^{(\alpha)}(\mathbf{r}-\mathbf{r}')d\mathbf{r}', \tag{10}$$

where the subscripts $\alpha=0$, 1, 2, 3, $V1$, $V2$ denote the index of six weight functions $w_j^{(\alpha)}(r)$; and $j=1,2$ stands for a polymeric segment (1) or a solvent molecule (2). The number density of segments $\rho_1(\mathbf{r})$ is given by

$$\rho_1(\mathbf{r})=\sum_{i=1}^{M}\rho_{si}(\mathbf{r})=\sum_{i=1}^{M}\int d\mathbf{R}\,\delta(\mathbf{r}-\mathbf{r}_i)\rho_M(\mathbf{R}), \tag{11}$$

where $\rho_{si}(\mathbf{r})$ stands for the local density of segment i.

Among the six weight functions, three are directly related to the geometry of a spherical particle:

$$w_j^{(2)}(r)=\delta(\sigma_j/2-r), \tag{12}$$

$$w_j^{(3)}(r)=\Theta(\sigma_j/2-r), \tag{13}$$

$$\mathbf{w}_j^{(V2)}(\mathbf{r})=(\mathbf{r}/r)\,\delta(\sigma_j/2-r), \tag{14}$$

where σ_j represents the diameter of a hard-sphere segment ($j=1$) or of a monomeric hard sphere ($j=2$); $\Theta(r)$ is the Heaviside step function, and $\delta(r)$ denotes the Dirac delta function. Integration of the two scalar functions, $w_j^{(2)}(r)$ and $w_j^{(3)}(r)$, with respect to position gives, respectively, the particle surface area and volume; and integration of the vector function $\mathbf{w}_j^{(V2)}(\mathbf{r})$ is related to the gradient across a sphere in the $\mathbf{r}$ direction. The other weight functions in FMT are proportional to the three geometric functions

$$w_j^{(0)}(r)=\frac{w_j^{(2)}(r)}{\pi\sigma_j^2},\quad w_j^{(1)}(r)=\frac{w_j^{(2)}(r)}{2\pi\sigma_j},$$
$$\mathbf{w}_j^{(V1)}(r)=\frac{\mathbf{w}_j^{(V2)}(r)}{2\pi\sigma_j}. \tag{15}$$

All weight functions are independent of the density profiles.

Using the scaled-particle differential equation, Rosenfeld derived the excess Helmholtz energy density due to hard-sphere repulsion[37]

$$\Phi^{\mathrm{hs}}\{n_\alpha(\mathbf{r})\}=\Phi_1^{\mathrm{hs}}+\Phi_2^{\mathrm{hs}}+\Phi_3^{\mathrm{hs}}, \tag{16a}$$

where

$$\Phi_1^{\mathrm{hs}}=-n_0\ln(1-n_3), \tag{16b}$$

$$\Phi_2^{\mathrm{hs}}=\frac{n_1n_2-\mathbf{n}_{V1}\cdot\mathbf{n}_{V2}}{(1-n_3)}, \tag{16c}$$

$$\Phi_3^{\mathrm{hs}}=\frac{\frac{1}{3}n_2^3-n_2\mathbf{n}_{V2}\cdot\mathbf{n}_{V2}}{8\pi(1-n_3)^2}. \tag{16d}$$

In the limit of a bulk fluid, the two vector weighted densities $\mathbf{n}_{V1}$ and $\mathbf{n}_{V2}$ vanish, and the Helmholtz energy becomes identical to that from the Percus–Yevick equation or from the scaled-particle theory.[38]

According to Wertheim's first-order perturbation theory for a bulk fluid, the Helmholtz energy density due to chain connectivity is given by

$$\Phi^{\mathrm{chain},b}=\frac{1-M}{M}\rho_{1b}\ln y_{11}^{\mathrm{hs},b}(\sigma_1), \tag{17}$$

where ρ_{1b} is the segment number density and $y_{11}^{\mathrm{hs},b}(\sigma_1)$ is the contact value of the cavity correlation function between segments, both in the bulk. To extend Eq. (17) to inhomogeneous systems, we assume that the weighted densities of FMT can be similarly applied to calculate the Helmholtz energy density due to chain connectivity. However, as discussed in our previous work,[39] ρ_{1b} in Eq. (17) must be replaced by $n_{01}\zeta_1$ and $y_{11}^{\mathrm{hs},b}(\sigma_1)$ must be replaced by

$$y_{11}^{\mathrm{hs}}(\sigma_1,n_\alpha)=\frac{1}{1-n_3}+\frac{n_2\sigma_1\zeta}{4(1-n_3)^2}+\frac{n_2^2\sigma_1^2\zeta}{72(1-n_3)^3}, \tag{18}$$

where $\zeta_1=1-\mathbf{n}_{V21}\cdot\mathbf{n}_{V21}/n_{21}^2$ and $\zeta=1-\mathbf{n}_{V2}\cdot\mathbf{n}_{V2}/n_2^2$. Substitution gives the Helmholtz energy density due to chain formation at inhomogeneous conditions

$$\Phi^{\mathrm{chain}}(n_\alpha)=\frac{1-M}{M}n_{01}\zeta_1\ln y_{11}^{\mathrm{hs}}(\sigma_1,n_\alpha). \tag{19}$$

Equation (19) is different from that obtained from a local density approximation.

C. Euler–Lagrange equations

Minimization of the grand potential with respect to the density profiles yields the following Euler–Lagrange equations:

$$\rho_2(\mathbf{r})=\exp[\beta\mu_2-\beta\Psi_2(\mathbf{r})-\delta(\beta F_{\mathrm{ex}})/\delta\rho_2(\mathbf{r})], \tag{20a}$$

$$\rho_M(\mathbf{R})=\exp[\beta\mu_M-\beta V_b(\mathbf{R})-\beta\Psi_{\mathrm{ext}}(\mathbf{R})-\beta\Lambda(\mathbf{R})]. \tag{20b}$$

In Eq. (20b), $\Lambda(\mathbf{R})=\delta F_{\mathrm{ex}}/\delta\rho_M(\mathbf{R})$ represents an effective potential field due to intra- and intermolecular interactions. Using Eq. (11), this effective potential can be simplified to

$$\Lambda(\mathbf{R})=\frac{\delta F_{\mathrm{ex}}}{\delta\rho_M(\mathbf{R})}=\sum_{i=1}^{M}\frac{\delta F_{\mathrm{ex}}}{\delta\rho_1(\mathbf{r}_i)}. \tag{21}$$

Substituting Eq. (21) into Eq. (20b) yields

$$\rho_M(\mathbf{R}) = \exp\left\{ \beta\mu_M - \beta V_b(\mathbf{R}) - \beta\sum_{i=1}^{M} \lambda_i(\mathbf{r}_i) \right\}, \tag{22a}$$

where $\lambda_i(\mathbf{r}_i)$ is related to the excess Helmholtz energy F_{ex} and the external potential $\varphi_i(\mathbf{r}_i)$ by

$$\lambda_i(\mathbf{r}_i) = \frac{\delta F_{\text{ex}}}{\delta\rho_1(\mathbf{r}_i)} + \varphi_i(\mathbf{r}_i). \tag{22b}$$

Equation (22) indicates that the segment density is determined by the chain connectivity and an effective external potential $\lambda_i(\mathbf{r}_i)$ that is the same for all segments, as in a typical self-consistent-field theory.[6]

Introducing segment densities $\rho_{si}(\mathbf{r})$ to Eq. (22) yields a set of coupled integral equations

$$\rho_{si}(\mathbf{r}) = \int d\mathbf{R}\, \delta(\mathbf{r}-\mathbf{r}_i) \exp\left[\beta\mu_M - \beta V_b(\mathbf{R}) - \beta\sum_{j=1}^{M} \lambda_j(\mathbf{r}_j) \right]. \tag{23}$$

From Eqs. (4), (11), and (23), we derive the average segment density of chain molecules

$$\rho_1(\mathbf{r}) = \exp(\beta\mu_M) \int d\mathbf{R} \sum_{i=1}^{M} \delta(\mathbf{r}-\mathbf{r}_i) \exp\left[-\beta V_b(\mathbf{R}) - \beta\sum_{j=1}^{M} \lambda_j(\mathbf{r}_j) \right]. \tag{24}$$

Equations (20a) and (24) provide the key equations to calculate the density profiles of the polymer segments and solvent molecules.

D. Numerical method

We calculated segment density distributions and adsorption isotherms of hard-sphere chains near a planar hard wall or in slit-like hard pores with or without solvent hard spheres. To provide insights into colloidal forces due to nonadsorbing polymers, we also calculated the solvation forces between two hard walls separated by hard-sphere chains. We compared the calculated results with Monte Carlo simulation results whenever they are available.

For each chain segment (j) or a solvent molecule (2), the external potential due to a hard wall is

$$\varphi_i(z)$$

or

$$\Psi_2(z) = \begin{cases} \infty & z<0 \\ 0 & z>0, \end{cases} \tag{25}$$

where z represents the perpendicular distance from the wall. Similarly, when the mixture is confined in a slit-like hard pore of width H, the external potential is

$$\varphi_i(z)$$

or

$$\Psi_2(z) = \begin{cases} \infty & z<0 \text{ or } z>H \\ 0 & \text{otherwise.} \end{cases} \tag{26}$$

For systems with the density distributions changing only in z direction, $\rho_i(\mathbf{r}) = \rho_i(z)$, Eqs. (20a) and (24) can be simplified to

$$\rho_2(z) = \exp[\beta\mu_2 - \beta\Psi_2(z) - \delta(\beta F_{\text{ex}})/\delta\rho_2(z)], \tag{27}$$

$$\rho_1(z) = \exp(\beta\mu_M) \sum_{i=1}^{M} \exp[-\beta\lambda_i(z)] G^i(z) G^{M+1-i}(z), \tag{28}$$

where the function $G^i(z)$ is determined from the recurrence relation

$$G^i(z) = \int dz' \exp[-\beta\lambda_i(z')] \times \frac{\theta(\sigma_1 - |z-z'|)}{2\sigma_1} G^{i-1}(z'), \tag{29}$$

for $i = 2,\ldots,M$ with $G^1(z) = 1$.

The chemical potentials for solving the density profiles are obtained directly from Wertheim's TPT1 equation of state for bulk hard-sphere-chain fluids[21]

$$\beta\mu_2 = \ln\rho_{2b} + \beta\mu_2^{\text{hs}}(\rho_{1b},\rho_{2b}) + \frac{1-M}{M}\rho_{1b}\frac{\partial \ln y_{11}^{\text{hs},b}(\sigma_1,\sigma_2)}{\partial\rho_{2b}}, \tag{30a}$$

$$\beta\mu_M = \ln\rho_M + M\beta\mu_M^{\text{hs}}(\rho_{1b},\rho_{2b}) + (1-M)\left[\ln y_{11}^{\text{hs},b}(\sigma_1,\sigma_2) + \rho_{1b}\frac{\partial \ln y_{11}^{\text{hs},b}(\sigma_1,\sigma_2)}{\partial\rho_{1b}} \right], \tag{30b}$$

where $\rho_{1b} = M\rho_M$, ρ_{2b} and ρ_M are, respectively, the bulk densities of solvent and chain molecules, $\mu_{1,M}^{\text{hs}}$ is the excess chemical potential of corresponding hard spheres that is calculated from the scaled-particle theory.[40] Equations (30a) and (30b) are identical to Eqs. (27) and (28) when the external potentials are removed.

We apply the Picard-type iterative method to solve Eqs. (27) and (28).[39] The iteration starts with bulk densities for the density profiles of chain segments and solvent molecules. The effective fields $\lambda_i(z)$ and the function $G^i(z)$ are then updated using the recurrence relation (29). A set of new density profiles is obtained from Eqs. (27) and (28), which are then mixed with the previous results as new input. The iteration repeats until the percentage change is smaller than 0.01 at all points. The numerical integrations were performed using the trapezoidal rule with step size $\Delta z = 0.02\sigma$.

III RESULTS AND DISCUSSION

A. Density profiles of hard-sphere chains near a hard wall or in slit pores

Figure 1 compares the calculated density profiles for hard-sphere 20-mers near a hard wall with Monte Carlo simulation data from Yethiraj and Hall.[41,42] Here the packing fraction of chain segments in the bulk is $\eta_b = \pi\rho_b\sigma^3/6 = 0.1$. In Fig. 1 and all subsequent figures, the density profiles are normalized by the bulk value ρ_b (or the average density in the pore ρ_{av}) and the perpendicular distance from the wall is given in units of σ. Also included in Fig. 1 are the

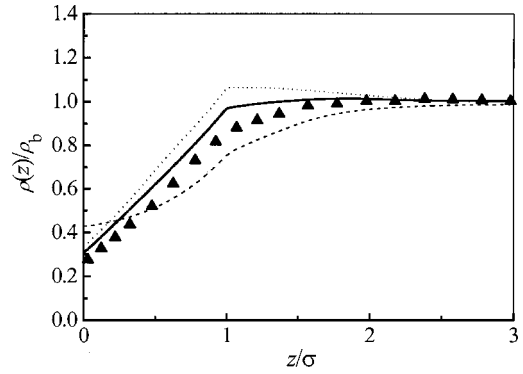

FIG. 1. The density profiles of hard sphere 20-mers near a hard wall at $\eta_b=0.1$. Symbols represent simulation results (Refs. 41 and 42), the solid line is from this work, the dotted line is from KR theory (Ref. 19), and the dashed line is from the integral-equation theory by Yethiraj and Hall (Ref. 11).

theoretical predictions from the Kierlik and Rosinberg (KR) theory[19] and from an integral-equation theory by Yethiraj and Hall.[11] While all theoretical predictions show correct surface depletion, the present theory agrees best with the simulation results. At low density, the depletion of polymer chains is because the polymer configurations are restricted in the region near the wall. The contact density predicted by the present theory is slightly lower than that given by the KR theory because in the calculation of the Helmholtz energy functional due to chain connectivity, we use the Carnahan–Starling equation instead of the Percus–Yevick solution for the contact value of the cavity correlation function of hard spheres.[38]

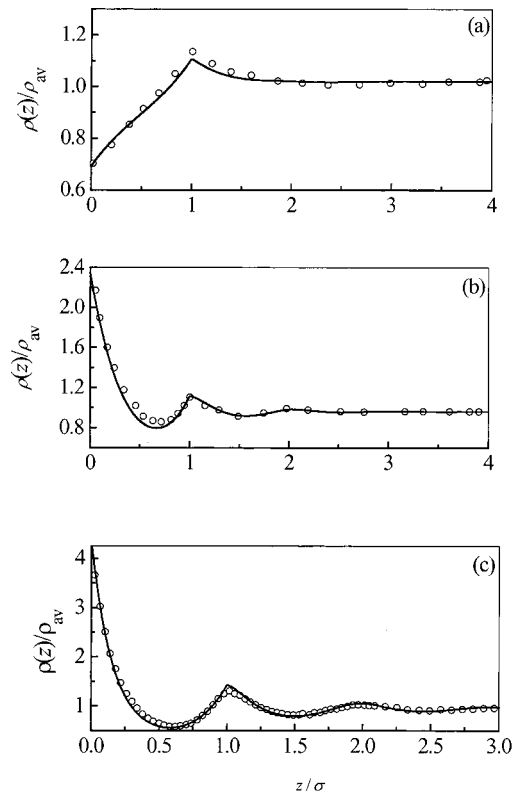

FIG. 2. The segment-density profiles from theoretical predictions (solid line) and from Monte Carlo simulations (symbols)—Ref. 19—for hard-sphere trimers in a slit hard pore of width $H=10\sigma$. The average packing fractions are (a) $\eta_{av}=0.1$, (b) $\eta_{av}=0.3$, and (c) $\eta_{av}=0.4$.

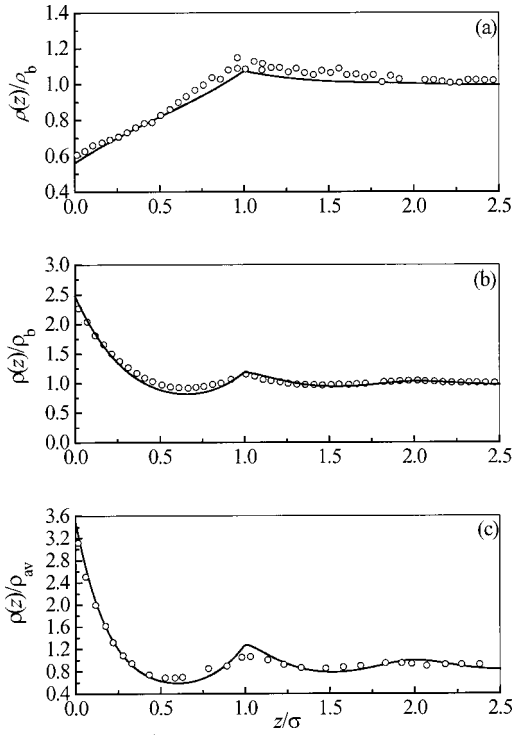

FIG. 3. The segment-density profiles from theoretical predictions (solid line) and from Monte Carlo simulation—Refs. 41 and 42 (symbols) for hard-sphere 4-mers in a slit hard pore of width $H=10\sigma$. The average packing fractions are (a) $\eta_{av}=0.1$, (b) $\eta_{av}=0.3$, and (c) $\eta_{av}=0.4$.

Figures 2–4 compare the calculated density profiles with Monte Carlo simulation data for hard-sphere chains confined between hard walls. Three chain lengths are considered, $M=2$, 4, and 20. Our theory precisely captures the transition from depletion to adsorption as the chain density increases. At high chain density, the distribution of segments resembles that for a monomeric fluid because in this case, the distribution depends primarily on hard-sphere packing. The cusp at $z=\sigma$ reflects the discontinuity of the wall-chain potential. Even though the current method is simpler than previous versions of DFTs for hard-sphere chains,[17,19,27] it provides as good as or better agreement with simulation results.

Figure 5 shows the density profiles for 100-mers in a slit pore. Here the pore width is $H=10\sigma$ and the bulk packing fractions are $\eta_b=0.025$, 0.1, and 0.2. At $\eta_b=0.025$, the hard-sphere chains are essentially independent of each other. In this case, the depletion persists over a distance approximately equal to the root-mean-square radius of gyration of a single chain. As density increases, the packing effect becomes more important and the density profile starts to oscillate at $\eta_b=0.2$.

B. End and middle segment distributions

Figures 6(a) and 6(b) compare the density profiles of the end and the middle segments for hard-sphere 20-mers in a hard slit pore with pore width $H=16\sigma$. Two packing fractions are considered, $\eta_{av}=0.1$ and 0.3. Because of chain con-

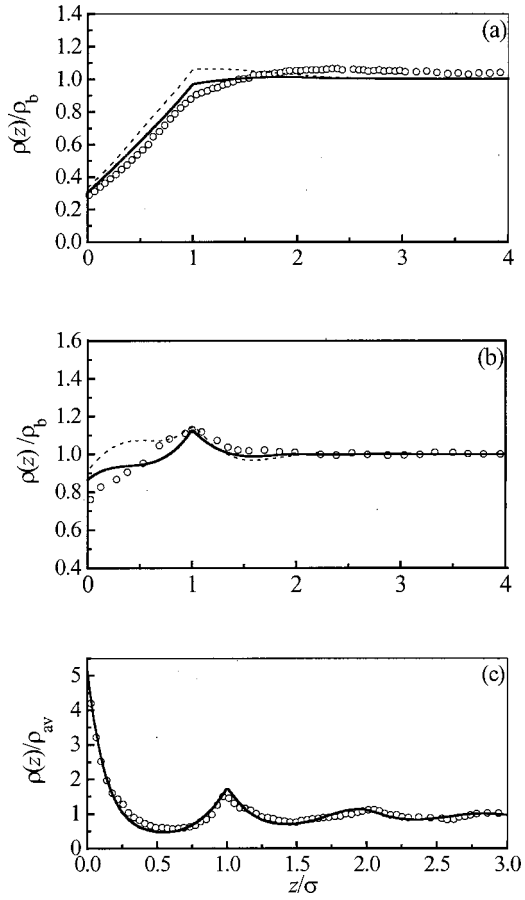

FIG. 4. The average density profiles from theoretical predictions and from Monte Carlo simulation (Refs. 28 and 42) for hard-sphere 20-mers. The pore width and average packing fractions are (a) $H=16\sigma$, $\eta_{av}=0.1$, (b) $H=16\sigma$, $\eta_{av}=0.2$, and (c) $H=10\sigma$, $\eta_{av}=0.45$. The symbols and lines have the same meaning as those in Fig. 2. The dashed lines are from KR theory (Ref. 19).

nectivity, the end and the middle segment distributions are dramatically different. At both packing fractions, the end-segment density near the wall is greater than that for the middle segments. Similar results have been found in the neutron-reflectivity experiments for polymer melts.[43] Preferential adsorption of end segments is because the wall has

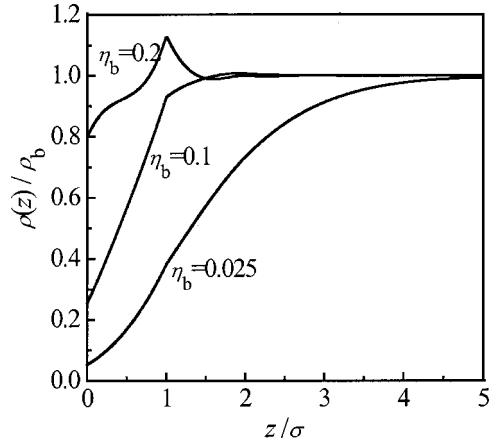

FIG. 5. The density profiles of 100-mers in a slit pore with width $H=10\sigma$ at bulk packing fractions $\eta_b=0.025$, 0.1, and 0.2.

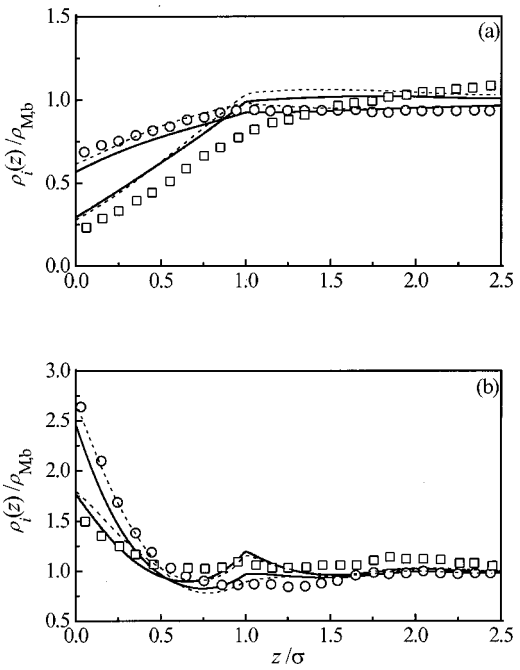

FIG. 6. The end- and middle-segment densities of hard-sphere 20-mers in a slit pore with width $H=16\sigma$. Open circles and open squares represent, respectively, simulation results (Ref. 42) for the end and middle segment, solid lines are predictions from this work, the dashed lines are from the KR theory (Ref. 19). The average packing fractions are (a) $\eta_{av}=0.1$; (b) $\eta_{av}=0.3$.

smaller effect on the chain configuration when it is in contact with the end segments compared with that when it is contact with the middle segments. Because the KR theory[19] uses the inhomogeneous cavity correlation function for representing chain connectivity, it gives slightly better density distributions for the end and the middle segments.

C. Partitioning coefficient and surface excess

The adsorption of hard-sphere chains in a slit pore of width H is characterized by the partitioning coefficient defined as

$$K_c=\rho_{av}/\rho_b, \tag{31}$$

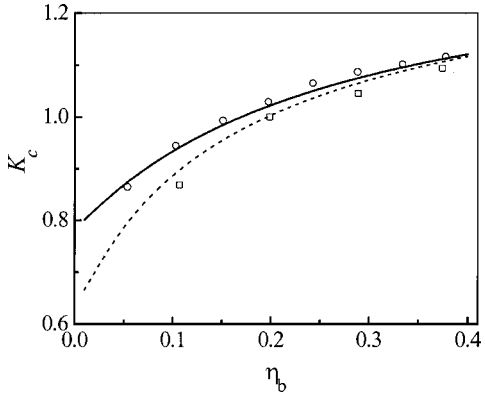

FIG. 7. The partitioning coefficient as a function of bulk volume fraction for hard-sphere 4-mers (open circles and solid line) and 8-mers (open squares and dash line) in a slit pore with width $H=5\sigma$. The symbols represent simulation results (Refs. 41 and 42) and the lines represent predictions from this work.

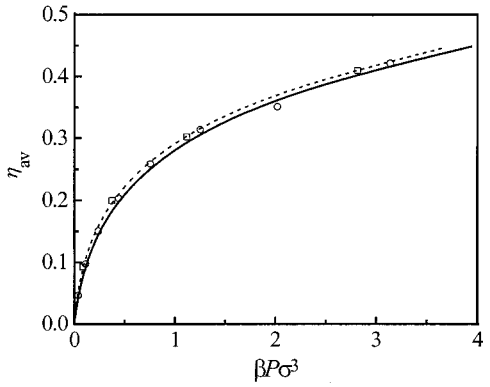

FIG. 8. Adsorption isotherms of 4-mers and 8-mers in a slit pore with width $H=5\sigma$. The notations are the same as those in Fig. 7.

where ρ_b is the bulk density and the average density in the pore ρ_{av} is given by

$$\rho_{av}=\frac{1}{H}\int_0^H \rho(z)dz. \tag{32}$$

For hard-sphere chains near a hard wall, the surface excess Γ is defined as

$$\Gamma=\int_0^\infty [\rho(z)-\rho_b]dz. \tag{33}$$

Figure 7 shows the calculated partitioning coefficient K_c for hard-sphere 4-mers and 8-mers as a function of the bulk volume fraction η_b at pore width $H=5\sigma$. Figure 8 gives the corresponding adsorption isotherms. For both cases, the theory agrees favorably with the simulation data.[41,42]

Figure 9 presents the surface excesses of hard-sphere 20-mers near a hard wall from theory and simulations. Due to chain connectivity, the surface excess exhibits a minimum at intermediate density. Interestingly, the adsorption of hard-sphere chains on a hard wall is qualitatively similar to that for strongly associating hard-sphere fluids.[39] Our predictions for the surface excesses are in good agreement with those from CMS-DF theory of Hooper *et al.* and with the results of simulation.[35]

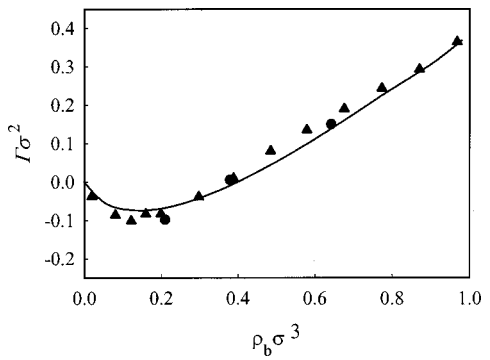

FIG. 9. Surface excess as a function of bulk density. Closed circles and triangles represent Monte Carlo results from Yethiraj (Refs. 28, 41, 42) and from Hooper *et al.* (Ref. 33), respectively. The solid line is the prediction from this work.

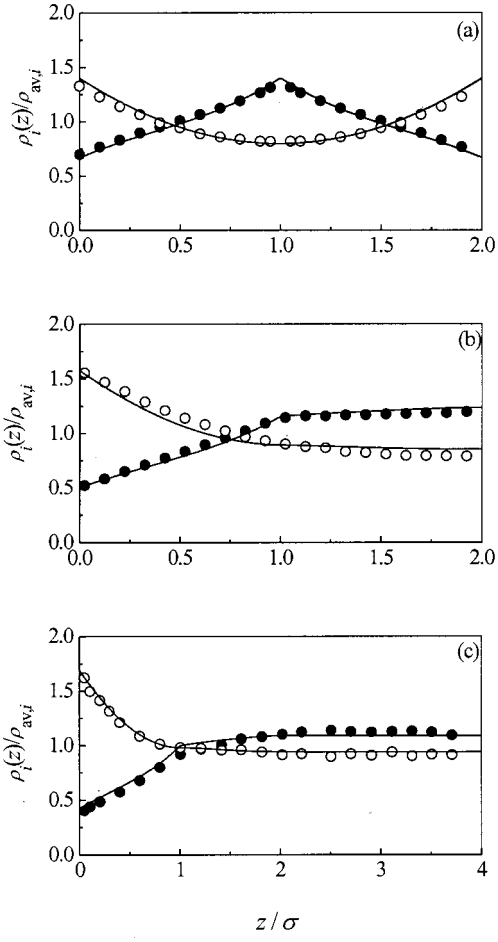

FIG. 10. Comparison between theory and Monte Carlo simulations (Ref. 46) for the density profiles to an equal molar mixture of hard-sphere 8-mers and monomers at $\eta_{av}=0.12$. The slit-pore widths are (a) $H=2\sigma$, (b) $H=4\sigma$, and (c) $H=10\sigma$. The open circles refer to Monte Carlo data for hard spheres, the closed circles are Monte Carlo data for 8-mers and the solid lines are calculated from this work.

D. Density profiles of chain-sphere mixtures

We consider equal molar mixtures of hard-sphere 8-mers and monomers confined in slit pores. Theoretical predictions are compared with Monte Carlo simulation data[28] for three pore widths ($H=2\sigma$, 4σ, and 10σ) and two packing fractions ($\eta_{av,1}=\eta_{av,2}=0.06$ and 0.172). Figure 10 shows that when the average packing fraction is small ($\eta_{av,1}=\eta_{av,2}=0.06$), the monomer density decays monotonically from the wall, while the opposite is true for the segment density. The drastic difference is again due to the effect of wall on chain configurations. As the average density increases ($\eta_{av,1}=\eta_{av,2}=0.172$, see Fig. 11), both segment and monomer density profiles exhibit a maximum at the wall. In this case, the density distributions are dominated by the packing effect. A comparison of Figs. 10 and 11 indicates that at low volume fraction, both chain and monomer densities at the wall are insensitive to the change in pore width. However, at higher packing fraction, while the wall density for the chain remains insensitive with pore width, the monomer density at the wall increases significantly as the pore width increases.

Figures 12(a) and 12(b) present the density profiles for the end and the middle segments of hard-sphere 8-mers in

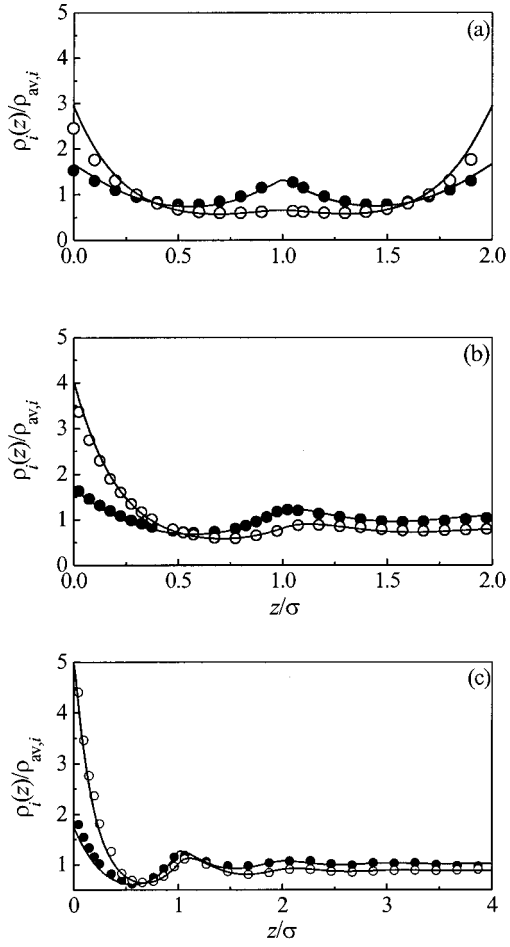

FIG. 11. Same as Fig. 10 but $\eta_{av}=0.344$.

those mixtures considered in Figs. 10 and 11. Here the pore width is $H=4\sigma$. Similar to that for the single component hard-sphere chains confined in slit pores (Fig. 6), the density of the end segments near the wall is greater than that for the middle segments.

E. Solvation forces

The force between two hard walls separated by a hard-sphere-chain fluid can be calculated from the contact value theorem[2]

$$F_H/(2AkT)=\rho(0), \tag{34}$$

where F_H/A is the force per unit area on a single wall and $\rho(0)$ is the contact segment density. A factor of 2 in Eq. (34) is introduced because A is defined as the area of a single wall. The solvation force per unit area is given by $F_s=F_H-F_\infty$, where F_∞ is the force per unit area when the walls are infinitely apart. For hard-sphere chains, the solvation force per area can be calculated from

$$F_s/(2AkT)=\rho(0)-\rho_\infty(0), \tag{35}$$

where $\rho_\infty(0)$ is the site density at the wall when the pore width is $H=\infty$.

We calculated the solvation forces between two hard walls separated by hard-sphere 4-mers and 100-mers. Figures 13(a)–(c) present the force profiles at three bulk packing

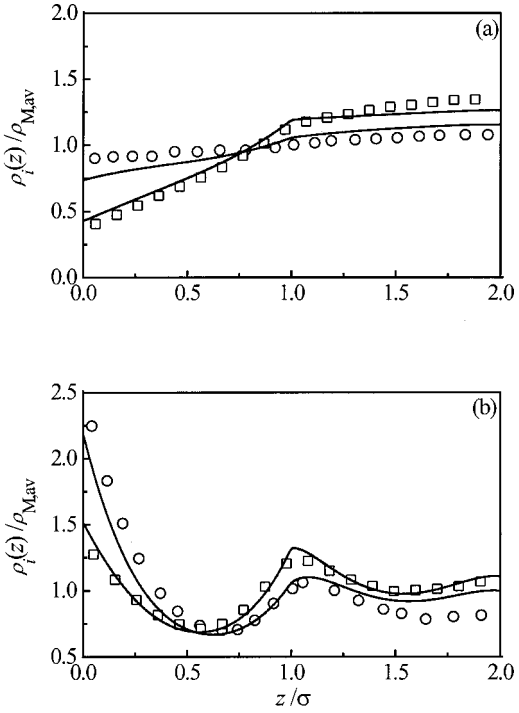

FIG. 12. The end- and middle-segment density profiles of hard-sphere 8-mers in equal molar mixtures with hard spheres in confined in a slit pore of width $H=4\sigma$. The average packing fractions are (a) $\eta_{av}=0.12$ and (b) $\eta_{av}=0.344$. The open circles and squares represent, respectively, Monte Carlo data (Ref. 46) for end and middle segments, and the solid lines are the predictions from this work.

fractions, $\eta_b=0.1$, 0.2, and 0.3. Figure 13(a) shows that at low chain density, the solvation force is attractive and decays monotonically toward zero, in consistence with the density profiles shown in Figs. 3(a) and 5. At modest density, the density profile of hard-sphere chains confined in a slit pore exhibits a peak out of the depletion zone [see Figs. 3(b), 4(b), and 5], leading to a similar peak in the solvation force [Fig. 13(b)]. It is interesting to note that at moderate density a repulsive barrier occurs prior to the attractive depletion region. At high density, the solvation force oscillates with a periodicity close to the segment diameter. Figure 13(c) indicates that the chain length has little effects on the solvation force at high densities, as predicted by the polymer scaling theories.[6] Figure 13 shows that the polymer-mediated solvation forces are much more complicated than that given by the simplistic Asakura–Oosawa theory.[44] The results shown in Fig. 13 are in qualitative agreement with integral-equation theory,[10] CMS-DF theory of McCoy *et al.*,[36] and the surface-force measurements for the force between mica surfaces separated by linear alkanes or in polydimethylsiloxane (PDMS).[45]

IV. CONCLUSIONS

We have shown that the fundamental-measure theory of Rosenfeld for inhomogeneous hard spheres and Wertheim's thermodynamic perturbation theory for bulk hard-sphere chains can be combined to represent the nonideality of inhomogeneous polymeric fluids due to excluded volume effects and chain connectivity. The new density functional has been tested with extensive Monte Carlo simulation data for the

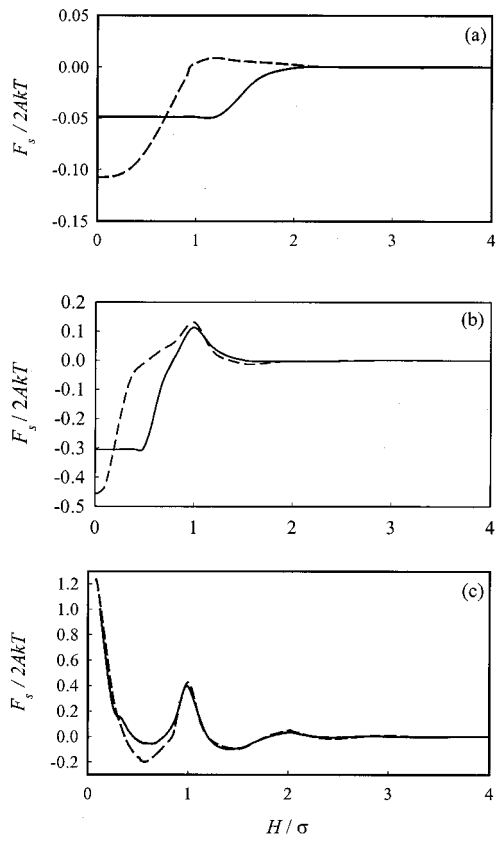

FIG. 13. Calculated solvation forces between two hard walls separated by hard-sphere chains. The bulk packing fractions are (a) $\eta_b = 0.1$, (b) $\eta_b = 0.2$, and (c) $\eta_b = 0.3$. The dashed lines are for 4-mers and the solid lines are for 100-mers.

segment density distributions and adsorption isotherms. Once van der Waals attractions are included, this new theory will be useful to describe structural and thermodynamic properties of inhomogeneous polymeric fluids and colloidal forces due to nonadsorption polymers.

We also calculated the solvation forces between two parallel walls separated by hard-sphere chain fluids. At low chain density, the solvation force is attractive due to the depletion of chain molecules from the surface and it decays monotonically with separation. At intermediate chain density, the solvation force shows a maximum repulsion approximately at one-segment diameter. At high densities, the solvation force is an oscillatory function of wall separation H with a periodicity approximately equal to the segment diameter. These features are not captured by the conventional Asakura–Oosawa theory for polymer mediated interactions but they are qualitatively consistent with experimental measurements and integral-equation calculations.

ACKNOWLEDGMENTS

This work is supported by a grant from the UC Energy Research Institute and by an initial compliment for J.W. from the University of California at Riverside.

[1] D. F. Evans and H. Wennerström, *The Colloidal Domain: Where Physics, Chemistry, Biology, and Technology Meet*, 2nd ed. (Wiley-VCH, New York, 1999).
[2] J. N. Israelachvili, *Intermolecular and Surface Forces*, 2nd ed. (Academic, London, 1992).
[3] J. Mahanty and B. W. Ninham, *Dispersion Forces* (Academic, London, 1976).
[4] K. F. Freed, *Renormalization Group Theory of Macromolecules* (Wiley, New York, 1987); W. E. McMullen and K. R. Freed, J. Chem. Phys. **92**, 1413 (1990).
[5] G. J. Fleer, M. A. Cohen-Stuart, and J. M. H. M. Scheutjens, *Polymers at Interfaces* (Chapman & Hall, London, 1993).
[6] P. G. de Gennes, *Scaling Concepts in Polymer Physics* (Cornell University Press, Ithaca, NY, 1979).
[7] K. Binder, Adv. Polym. Sci. **138**, 1 (1999).
[8] I. C. Sanchez, *Physics of Polymer Surfaces and Interfaces* (Butterworth–Heinemann, Stoneham, MA, 1992).
[9] Y. Duda, D. Henderson, A. Trokhymchuk, and D. Wasan, J. Phys. Chem. B **103**, 7495 (1999).
[10] D. Henderson, A. Kovalenko, O. Pizio, and D. Wasan, Physica A **245**, 276 (1997).
[11] A. Yethiraj and C. K. Hall, J. Chem. Phys. **95**, 3749 (1991).
[12] K. Schweizer, Adv. Chem. Phys. **XCVIII**, 1 (1997).
[13] D. Chandler, J. D. McCoy, and S. J. Singer, J. Chem. Phys. **85**, 5971 (1986).
[14] D. Chandler, J. D. McCoy, and S. J. Singer, J. Chem. Phys. **85**, 5977 (1986).
[15] J. D. McCoy, S. J. Singer, and D. Chandler, J. Chem. Phys. **87**, 4853 (1987).
[16] R. Evans, in *Fundamentals of Inhomogeneous Fluids*, edited by D. Henderson (Dekker, New York, 1992), pp. 85–175.
[17] J. B. Hooper, M. T. Pileggi, J. D. McCoy, J. G. Curro, and J. D. Weinhold, J. Chem. Phys. **112**, 3094 (2000).
[18] C. E. Woodward, J. Chem. Phys. **94**, 3183 (1991).
[19] E. Kierlik and M. L. Rosinberg, J. Chem. Phys. **100**, 1716 (1994).
[20] D. Chandler and L. R. Pratt, J. Chem. Phys. **65**, 2925 (1976).
[21] M. S. Wertheim, J. Chem. Phys. **87**, 7323 (1987).
[22] E. A. Muller and K. E. Gubbins, Ind. Eng. Chem. Res. **40**, 2193 (2001).
[23] Y. Hu, H. L. Liu, and W. C. Wang, Fluid Phase Equilib. **160**, 59 (1999).
[24] K. P. Shukla and W. G. Chapman, Mol. Phys. **91**, 1075 (1997).
[25] P. K. Jog and W. G. Chapman, Mol. Phys. **97**, 307 (1999).
[26] B. Q. Wang, J. Cai, H. L. Liu, and Y. Hu, Chin. J. Chem. Eng. **9**, 156 (2001).
[27] A. Yethiraj and C. E. Woodward, J. Chem. Phys. **102**, 5499 (1995).
[28] A. Yethiraj, J. Chem. Phys. **109**, 3269 (1998).
[29] J. D. McCoy, K. G. Honnell, K. S. Schweizer, and J. G. Curro, J. Chem. Phys. **95**, 9348 (1991).
[30] S. K. Nath, J. D. McCoy, J. G. Curro, and R. S. Saunders, J. Chem. Phys. **106**, 1950 (1997).
[31] J. D. McCoy, S. K. Nath, J. G. Curro, and R. S. Saunders, J. Chem. Phys. **108**, 3023 (1998).
[32] S. K. Nath, P. F. Nealey, and J. J. de Pablo, J. Chem. Phys. **110**, 7483 (1999).
[33] J. B. Hooper, J. D. McCoy, and J. G. Curro, J. Chem. Phys. **112**, 3090 (2000).
[34] S. Zhou and X. Zhang, Phys. Rev. E **64**, 011112 (2001).
[35] J. B. Hooper, J. D. McCoy, J. G. Curro, and F. van Swol, J. Chem. Phys. **113**, 2021 (2000).
[36] J. D. McCoy, M. A. Teixeira, and J. G. Curro, J. Chem. Phys. **114**, 4289 (2001).
[37] Y. Rosenfeld, Phys. Rev. Lett. **63**, 980 (1989).
[38] J. P. Hansen and I. R. McDonald, *Theory of Simple Liquids*, 2nd. ed. (Academic, London, 1990).
[39] Y.-X. Yu and J. Wu, J. Chem. Phys. **116**, 7094 (2002).
[40] Y. Rosenfeld, J. Chem. Phys. **89**, 4272 (1988).
[41] A. Yethiraj and C. K. Hall, Mol. Phys. **73**, 503 (1991).
[42] A. Yethiraj and C. K. Hall, Macromolecules **23**, 1865 (1990).
[43] W. Zhao, X. Zhao, M. H. Rafailovich *et al.*, Macromolecules **26**, 561 (1993).
[44] J. Z. Wu, D. Bratko, H. W. Blanch, and J. M. Prausnitz, J. Chem. Phys. **111**, 7084 (1999).
[45] M. L. Gee, T. Penger, J. N. Israelachvili, and T. A. Witten, J. Chem. Phys. **93**, 6057 (1990).
[46] A. Yethiraj and C. K. Hall, J. Chem. Phys. **91**, 4827 (1989).